ACS OMEGA

Open Access



http://pubs.acs.org/journal/acsodf

Article

# Synthesis of Ethylene Carbonate by Urea Transesterification Using Zeolitic Imidazolate Framework Derived Fe-Doped ZnO Catalysts

Sumin Lee, Hyun Joo Lee, Seung Hwan Chung, Je Seung Lee, and Sung Yul Lim*

Cite This: *ACS Omega* 2023, 8, 48704−48710

Read Online

ACCESS | Metrics & More | Article Recommendations | Supporting Information

**ABSTRACT:** The development of environmentally friendly and efficient methods for the synthesis of ethylene carbonate (EC) is crucial for advancing carbon capture, utilization, and storage technologies. Herein, we present the synthesis of EC through the transesterification of urea with ethylene glycol (EG) using a zeolitic imidazolate framework (ZIF) derived Fe-doped ZnO catalyst (Fe;ZnO−ZIF). The Fe;ZnO−ZIF catalyst, prepared by incorporating Fe dopant atoms into a ZnO−ZIF template, demonstrates excellent catalytic activity, achieving high conversion of reactants and superior selectivity toward EC at 160 °C for 150 min under an applied vacuum (160 mmHg). Based on the thermogravimetric, X-ray spectroscopic, and temperature-programmed desorption analysis, the simultaneous presence of strong Lewis acidic and basic sites in Fe;ZnO-ZIF enables its excellent catalytic performance toward EC synthesis with high selectivity. Acidic sites activate the carbon center in urea, while basic sites facilitate the nucleophilic attack on urea by deprotonation of EG. This synergistic reaction pathway resulting from the interaction between the strong Lewis acidic and basic sites promotes nucleophilic attacks of EG on urea, leading to significantly higher conversion efficiency and selectivity, compared to the commercial benchmark ZnO. Although the establishment of a continuous reaction system which takes into account cyclability and stability of the catalysts is further required in the future, our research reported herein provides valuable insights into the design of synergistic, localized active sites for EC synthesis and contributes to the development of sustainable carbon utilization technologies for achievement of net-zero emissions.

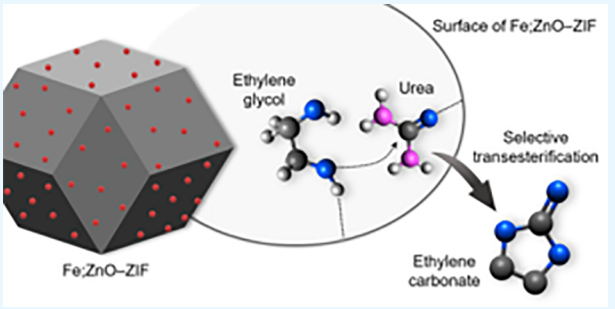


## 1. INTRODUCTION

Carbon dioxide ($CO_2$) is one of the most notorious greenhouse gases that has been ascribed as a serious issue in global warming. Consequently, the development of technologies for carbon capture, utilization, and storage has attracted considerable interest as a viable route to achieving carbon neutrality. There are currently two main strategies for $CO_2$ utilization: a direct approach (such as electrochemical $CO_2$ reduction) and an indirect approach that involves the utilization of chemicals derived from $CO_2$ for the synthesis of valuable products.[1] Among the various chemicals for the indirect approach, cyclic carbonates can be potentially used as environmentally friendly polar aprotic solvents for a wide range of compounds. Cyclic carbonates, especially ethylene carbonate (EC), are utilized as electrolytes in Li-ion batteries owing to their high dielectric constant and electrical conductivity.[2] Moreover, EC is a versatile and reactive chemical that serves as a valuable starting material and intermediate in various chemical processes, including selective alkoxylation and carbamate formation. These reactions enable the production of important compounds such as glycerol carbonate and linear carbonates like dimethyl carbonate.[3] Moreover, EC has attracted significant attention as a green solvent, a substitute for phosgene, and a fuel additive.[4]

Numerous studies of EC synthesis have been reported. One of the synthetic methods involves the reaction of phosgene with a diol, resulting in a high yield due to the high reactivity of phosgene.[5,6] However, phosgene and its byproducts are extremely toxic compounds, which has driven the search for safer alternatives. Another method is based on the utilization of epoxides and $CO_2$, which exhibit nearly complete conversions.[7−9] However, epoxides are difficult to handle on a large scale, because of their high toxicity and explosive nature. Furthermore, epoxides, such as ethylene oxide and propylene oxide, typically stem from fossil-fuel-derived sources, thereby conflicting with the goal of carbon neutrality. Therefore, alternative routes for the large-scale synthesis of EC must be developed to overcome these problems. Recently, the transesterification of ethylene glycol (EG) with urea has been proposed as a viable approach. This method has several

Received: July 13, 2023
Revised: October 13, 2023
Accepted: November 20, 2023
Published: December 14, 2023

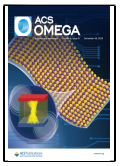

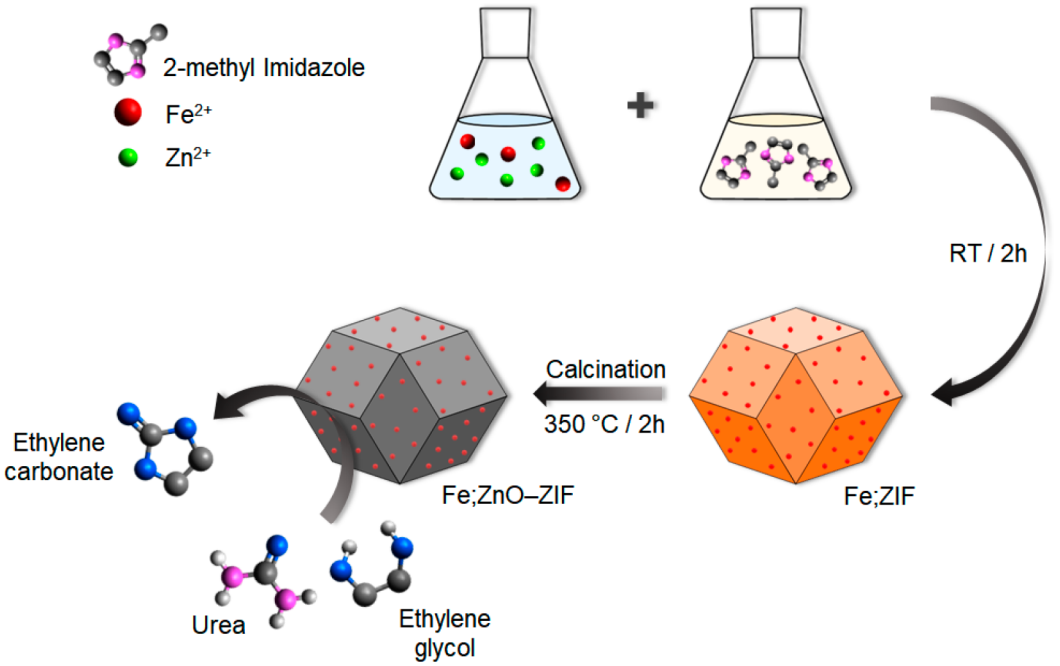


**Figure 1.** Schematic procedure for the fabrication of Fe;ZnO−ZIF.

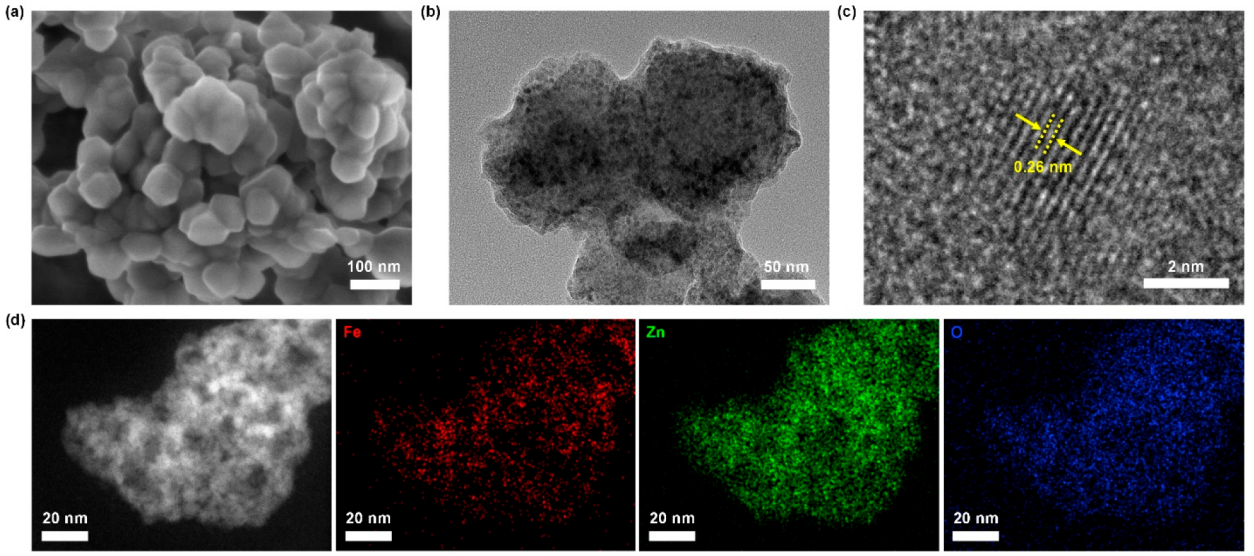


**Figure 2.** (a) SEM, (b) TEM, and (c) STEM images of Fe;ZnO−ZIF. (d) STEM-EDS mapping images of the Fe, Zn, and O elements in Fe;ZnO−ZIF.

advantages, including easy handling of the reactants, low toxicity, and a mild reaction environment. Additionally, urea can be produced through the reaction between $CO_2$ and ammonia ($NH_3$), indicating its potential contribution to the indirect $CO_2$ utilization for carbon neutrality. Li et al. conducted the same reaction over various catalysts, including CaO, $La_2O_3$, $ZrO_2$, $Al_2O_3$, MgO, and ZnO, and found that ZnO exhibited the highest activity and selectivity.[10] Jia and Zhao reported Al-containing and Fe-containing ZnO catalysts for urea transesterification.[11,12] Fakhrnasova investigated the mechanisms of acid−base catalyzed reactions by performing in situ dip-in attenuated total reflection infrared spectroscopic measurements.[4] Although various catalysts have been considered for this purpose, their conversion efficiency and selectivity should be further improved through the more efficient utilization of acidic and basic reactive sites based on an in-depth understanding of the catalytic reaction mechanism.

In this paper, we demonstrate the synthesis of EC via the transesterification of urea with EG catalyzed by a zeolitic imidazolate framework (ZIF) derived Fe-doped ZnO catalyst (Fe;ZnO−ZIF). A Zn ZIF (ZIF-8) was utilized as a template for ZnO−ZIF synthesis, which accommodated Fe dopant atoms owing to its porous structure, leading to a high catalytic activity.[13] The resultant Fe;ZnO−ZIF catalyst exhibited high conversion and selectivity toward EC, which is superior to that of pure ZnO−ZIF produced via the same method but without Fe incorporation. A surface analysis of Fe;ZnO−ZIF conducted using X-ray photoelectron spectroscopy (XPS) revealed that the high conversion efficiency and EC selectivity of this catalyst could be ascribed to the presence of Lewis basic


https://doi.org/10.1021/acsomega.3c05023
ACS Omega 2023, 8, 48704−48710

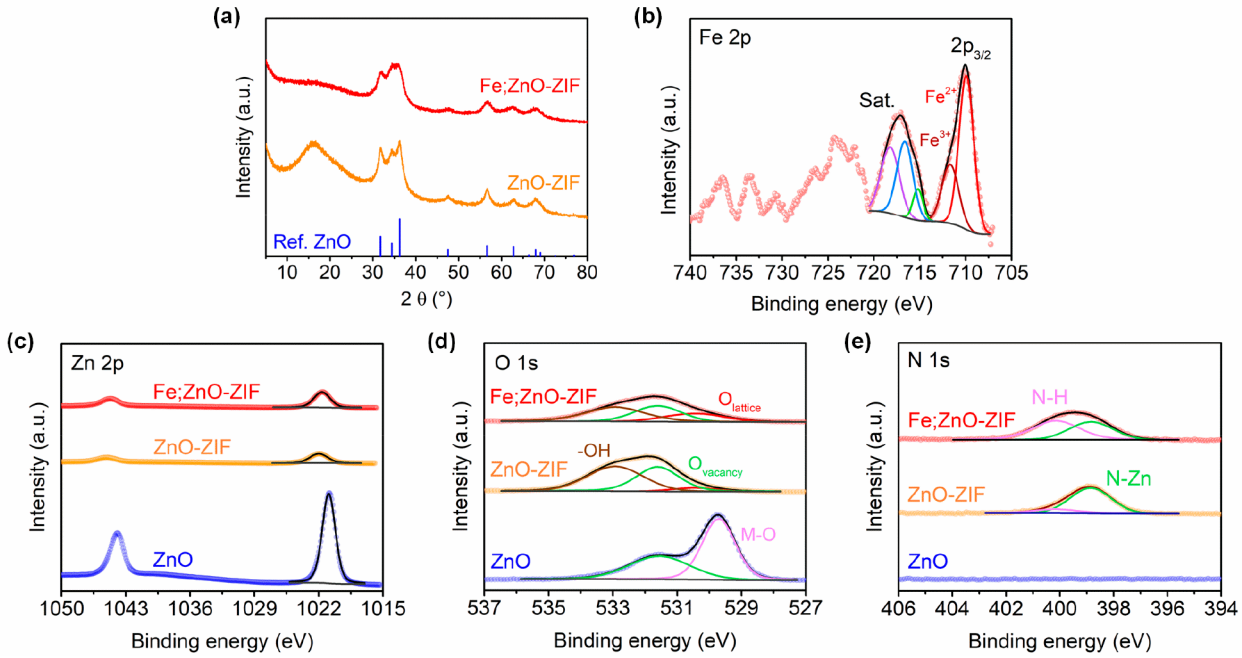


**Figure 3.** (a) XRD patterns of ZnO, ZnO-ZIF, and Fe;ZnO−ZIF. (b) Fe 2p XPS profile of Fe;ZnO−ZIF. XPS spectra of (c) Zn 2p, (d) O 1s, and (e) N 1s in ZnO, ZnO−ZIF, and Fe;ZnO−ZIF.

sites possibly originating from lattice oxygen on the ZnO surface and N−H sites in 2-methylimidazole (2-mIm) as well as Lewis acidic Zn sites from ZnO. The surface structure of Fe;ZnO−ZIF induced by Fe dopant improves the catalytic performance toward EC synthesis by pioneering a synergistic reaction pathway between these Lewis acidic and basic sites, facilitating nucleophilic attacks of EG molecules toward urea. Although detailed further investigation is required, especially from the perspective of stability for practical implementation of Fe;ZnO-ZIF catalysts, our findings suggest that an elaborate design of localized reactive sites is beneficial for the efficient catalysis of the target reaction.

## 2. RESULTS AND DISCUSSION

Figure 1 shows a scheme of the synthesis process of the catalyst Fe;ZnO-ZIF via a simple chemical approach followed by a thermal treatment. Detailed procedures are provided in the Experimental Section. Briefly, divalent metal ion solutions containing 150 mM $Zn^{2+}$ and 5 mM $Fe^{2+}$ were mixed with 600 mM of 2-mIm for 2 h under dark conditions. A 1:1 mixture of ethanol and methanol was used as the solvent throughout this process. The catalytic precursor particles Fe;ZIF were collected by centrifugation, followed by thermal treatment at 350 °C for 2 h to prepare the Fe;ZnO−ZIF. The thermal stability of Fe;ZIF was assessed through thermal gravimetric analysis (TGA) and compared to that of pure ZIF particles (Figure S1). Drastic changes in weight loss occurred from ∼400 °C for both Fe;ZnO−ZIF and ZnO−ZIF, with a miniscule weight loss being observed at 350 °C, which was the temperature employed to synthesize the catalysts. Especially, only 5.6% of the weight is reduced in Fe;ZnO−ZIF at 350 °C. This indicates that a temperature of 350 °C for the thermal treatment is insufficient to induce significant decomposition of the catalytic structures. Especially, the carbonization of 2-mIm, which is utilized as the ligand for $Zn^{2+}$, could not fully occur at 350 °C and is still located near the ZnO nanoparticles (NPs), thereby preserving the microporous structure of intrinsic ZIFs. Moreover, we also observed that the introduction of Fe into the catalyst further enhanced the thermal stability overall when compared to that without Fe (Figure S1).

The morphology of Fe;ZnO−ZIF was revealed via scanning electron microscopy (SEM) and transmission electron microscopy (TEM) (Figure 2). The images presented in Figure 2a,b indicate that the Fe;ZnO−ZIF catalyst shows rhombic dodecahedron like structures with diameters of approximately 80 nm.[14] In a high-resolution TEM image, ZnO NPs with sizes of ∼3 nm are highly dispersed in the catalyst. The interplanar distance in ZnO NPs (0.26 nm) corresponds to the *d* spacing of the (002) planes of ZnO with a hexagonal wurtzite structure (Figure 2c). Based on these TEM analyses, the heat treatment temperature for 350 °C is enough to induce the formation of ZnO while the ligand 2-mIm for ZIFs does not undergo significant structural decomposition when considering the aforementioned TGA results. The elemental maps obtained via a scanning TEM (STEM)-energy dispersive spectroscopic (EDS) analysis show the uniform distributions of Zn, Fe, and O elements throughout the Fe;ZnO−ZIF catalyst (Figure 2d). As the EDS signal of Fe atoms was much weaker than that of Zn atoms, the presence of Fe and Zn elements in Fe;ZnO-ZIF was confirmed by electron energy loss spectroscopy (Figure S2). Furthermore, inductively coupled plasma−mass spectrometry data revealed that the Fe/Zn atomic ratio in Fe;ZnO−ZIF is approximately 0.13, which was consistent with the weak Fe signal. However, a more detailed investigation of Fe atoms in the synthesized ZnO NPs was challenging because of the rapid degradation of the catalyst by exposure to the electron beam during STEM analysis.

The structural phases of the synthesized catalytic particles were studied by X-ray diffraction (XRD) (Figure 3a). When comparing the diffraction patterns of Fe;ZIF and Fe;ZnO−ZIF shown in Figure 3a and Figure S3, a distinctively different XRD pattern is acquired in Fe;ZnO−ZIF. This discrepancy indicates the successful formation of ZnO during the thermal treatment,


https://doi.org/10.1021/acsomega.3c05023
ACS Omega 2023, 8, 48704−48710

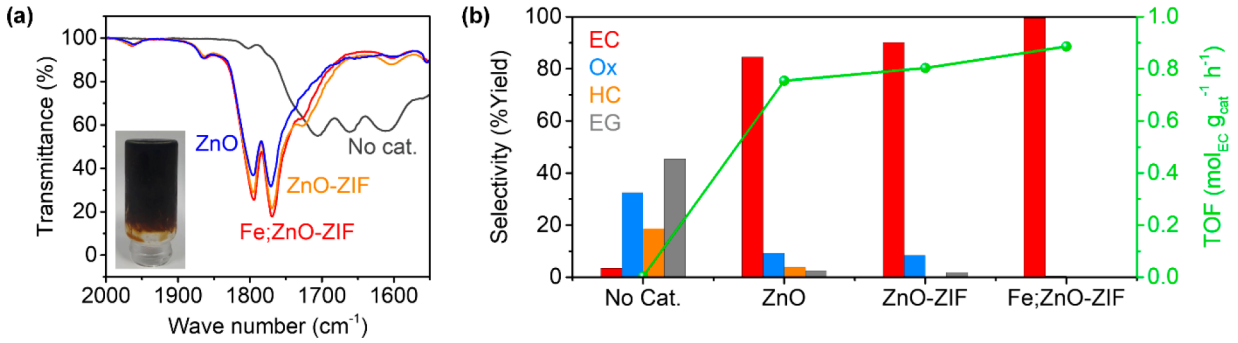


**Figure 4.** (a) IR spectra of the products after the urea transesterification with EG obtained without a catalyst and using commercial ZnO, ZnO−ZIF, and Fe;ZnO−ZIF catalysts. The inset shows a photograph of the product synthesized using the Fe;ZnO−ZIF catalyst. (b) Selectivity and TOF values obtained for the reactions conducted over commercial ZnO, ZnO−ZIF, and Fe;ZnO−ZIF. Each experiment was performed at 160 °C for 150 min under applied vacuum at 160 mmHg.

which is also confirmed by TEM images. The XRD pattern of Fe;ZnO−ZIF is well-matched with the hexagonal wurtzite structure (PDF #01-080-0075), consistent with the interplanar spacing determined through TEM observations (the red line in Figure 3a).[15] The peaks that originated from the ZnO crystalline structure are more prominent in the XRD pattern of ZnO−ZIF than in the Fe;ZnO−ZIF pattern (the orange line in Figure 3a). Although the ZnO peaks (especially those centered at 34 and 36°) slightly decreased after the introduction of Fe atoms, the overall pattern shape and peak positions remained unchanged. This implies that small amounts of Fe effectively replaced Zn atoms without significant structural deformation.

To obtain further structural information, XPS was conducted to determine the surface chemical states of the prepared catalysts. The Fe 2p spectrum displayed in Figure 3b confirms the presence of mixed oxidation states consisting of $Fe^{2+}$ and $Fe^{3+}$ in Fe;ZnO−ZIF. The Zn 2p spectra of commercial ZnO, ZnO−ZIF, and Fe;ZnO−ZIF are shown in Figure 3c. Compared with the Zn 2p peak positions of commercial ZnO, the peaks of ZnO−ZIF are shifted by 1.1 eV toward higher binding energies, implying that the electron density at the Zn sites in ZnO−ZIF is lower than that in commercial ZnO. Although a detailed reaction mechanism of the urea transesterification with EG remains incompletely elucidated, it is generally accepted that the Lewis acidity of Zn promotes the conversion into EC. As Lewis acidic Zn reduces the electron density of the carbon center in urea by interacting with the carbonyl group, this activated central carbon atom becomes electron-deficient, facilitating two sequential nucleophilic attacks by the hydroxyl group in EG. These sequential reactions lead to ring cyclization to form EC along with the concomitant production of $NH_3$. Indeed, ZnO−ZIF exhibited much higher catalytic activity toward EC synthesis compared to commercial ZnO, which is consistent with its lower electron density at the Zn sites reflected by the shift of the Zn 2p XPS peak toward higher energies.

As compared with the Zn 2p peaks of ZnO−ZIF, the Zn 2p spectrum of Fe;ZnO−ZIF is shifted toward lower binding energies by 0.3 eV, which apparently contradicts the transesterification mechanism discussed above. Thus, the lower Lewis acidity of Zn catalytic sites degrades the catalytic performance of Fe;ZnO−ZIF because the negative shift in the XPS profile indicates a higher electron density. However, the conversion into EC over Fe;ZnO−ZIF is unexpectedly higher than that over ZnO−ZIF, as discussed below.

The O 1s spectra of the studied catalysts are presented in Figure 3d. The O 1s spectrum of commercial ZnO exhibits typical oxygen-related chemical states that can be observed for other commercial ZnO catalysts. The ZIF−ZnO spectrum contains two deconvoluted peaks at 531.58 and 532.98 eV, which correspond to oxygen vacancies and −OH functional groups, respectively. However, the peak resulting from the lattice oxygen emerged after Fe was introduced into the ZnO−ZIF structure.[16] Considering the difference between the Zn 2p spectra of ZnO−ZIF and Fe;ZnO−ZIF, the newly formed lattice oxygen sites after Fe doping are likely responsible for the increased performance even with the peak shift toward lower binding energies. The presence of additional sites on the Fe;ZnO−ZIF surface with a high electron density at lattice oxygens could effectively reduce the binding energy of Zn.

Each peak in the N 1s spectra of ZnO−ZIF and Fe;ZnO−ZIF was deconvoluted into the peaks of N−H and N−Zn originating from 2-mIm ligands, which still remained near the ZnO NPs after the heat treatment (Figure 3e). However, a higher portion of the peak from N−H was observed in Fe;ZnO−ZIF compared to that in ZnO−ZIF. This phenomenon is also well-matched with the TGA results, indicating the improved thermal stability of Fe;ZnO−ZIF over ZnO−ZIF. N−H in 2-mIm is known to be vulnerable to thermal treatment due to its susceptibility to the oxidation process. Therefore, the increased N−H portion observed in XPS analysis can be rationalized by the enhanced thermal stability confirmed by TGA (Figure S1). As the N−H in 2-mIm is well-known to possess a high $pK_a$ value indicating its high basicity, we conclude from XPS analysis that both Lewis acidic (Zn) and basic (lattice oxygen and N−H in 2-mIm) sites together simultaneously exist in Fe;ZnO−ZIF.

Temperature-programmed desorption (TPD) studies using $CO_2$ and $NH_3$ were conducted to evaluate the Lewis basic and acidic sites in Fe;ZnO−ZIF, respectively. As shown in Figure S4a, commercial ZnO clearly exhibits two $CO_2$ desorption peaks at ∼220 and 380 °C, which are generally considered as moderately basic sites located at 200−400 °C. In ZnO−ZIF, the peak at ∼220 °C observed in ZnO is largely suppressed and the desorbed $CO_2$ signal is increased from ∼250 °C, implying a larger portion of stronger basic sites in ZnO−ZIF than those in ZnO. In Fe;ZnO−ZIF, the onset of desorption shifts further toward a higher temperature, indicating the existence of the strongest basic sites among the catalysts. A similar trend was also observed in the TPD measurements with $NH_3$, confirming the presence of both the strongest basic and


https://doi.org/10.1021/acsomega.3c05023
ACS Omega 2023, 8, 48704−48710

acidic sites in Fe;ZnO−ZIF among ZnO, ZnO−ZIF, and Fe;ZnO−ZIF (Figure S4b). Therefore, the coexistence of strong catalytic Lewis acidic and basic sites in Fe;ZnO−ZIF synergistically enhances its high catalytic performance toward EC formation, as illustrated in the proposed reaction mechanism shown in Figure S5.

The products of EC synthesis via the urea transesterification with EG using equal amounts of the commercial ZnO, ZnO−ZIF, and Fe;ZnO−ZIF catalysts were qualitatively analyzed by infrared (IR) spectroscopy (Figure 4a) after 150 min of reaction conducted under vacuum (160 mmHg) at 160 °C. As shown in the inset of Figure 4a, the obtained product solidified after cooling to 25 °C because of the high melting point of EC (approximately 36 °C). This complete solidification after transesterification implies the high conversion of EG and urea into EC, achieving 94% conversion efficiency as shown in Figure S6. Indeed, only the doublet peaks at 1795 and 1769 $cm^{-1}$, which correspond to the EC, are observed for Fe;ZnO−ZIF (red line in Figure 4a). The reaction duration is optimized at 150 min because the peak at 1725 $cm^{-1}$, originating from the formation of the byproduct 2-oxazolidone (2-Ox), is observed after 240 min of reaction (Figure S7). When the commercial ZnO (blue line in Figure 4a) and ZnO−ZIF (orange line in Figure 4a) catalysts are employed, the same doublet peaks are detected; however, their intensities are slightly lower than those of Fe;ZnO−ZIF. These results match the quantitative gas chromatography (GC) data presented in Figure 4b. The high conversion efficiency of Fe;ZnO−ZIF is also confirmed by the GC spectrum, which clearly indicates the near absence of EG, and only EC was observed as a distinct peak in the reaction mixture (Figure S8). In particular, side reactions often result in the formation of 2-Ox and 2-hydroxyethyl carbamate (HEC). However, the 2-Ox peak at 19.8 min is found to be negligible, and interestingly, the HEC peak, typically observed at 17.2 min, is completely absent in the case of using Fe;ZnO−ZIF. In summary, the highest conversion efficiency and selectivity toward EC are achieved using Fe;ZnO−ZIF as the catalyst. Furthermore, Fe;ZnO−ZIF shows the highest turnover frequency (TOF) of $8.86 \times 10^{-1}$ $mol_{EC}\ g_{cat}^{-1}\ h^{-1}$, which is about 10% and 20% higher than the values acquired from commercial ZnO and ZnO−ZIF, respectively, confirming the highest performance of Fe;ZnO−ZIF.

The acidic and basic sites in Fe;ZnO−ZIF for urea transesterification and their roles during urea transesterification are inferred based on TGA, XPS, and TPD analysis. As the acidity of Zn sites estimated from the peak position of Zn 2p in XPS analysis cannot fully support the higher selectivity toward EC in Fe;ZnO−ZIF than that in ZnO−ZIF, we consider the contribution of basic sites toward catalysis for the synergistic reaction pathway. Although the detailed surface structures of ZnO−ZIF and Fe;ZnO−ZIF have not been fully elucidated yet, the lattice oxygen and N−H sites could serve as the basic sites based on the XPS analysis. Currently, it remains uncertain which of these two basic sites has a more substantial role in contributing to the EC synthesis. When we conducted the experiment of urea transesterification with EG under the same reaction conditions with 2-mIm solely as the catalyst, which is known for having only Lewis base sites, a selectivity of 25.6% for EC, calculated from GC analysis, is achieved. The selectivity for EC using only ZnO, which is known for only Lewis acid sites, is 84.6%. Both of these EC selectivities for ZnO and 2-mIm are lower than that achieved using Fe;ZnO−ZIF (99.4%), as shown in Table S1, which contains both Lewis acidic and basic sites on the catalytic surface with proper distribution within the micropores originating from ZIF-based structures. This corroborates the fact that there could be a possibility of a synergistic reaction pathway between the acid and base sites as we suggested before (Figure S4). We postulate that while the Lewis acidic Zn activates the carbon center in urea by partially removing electron clouds, the deprotonated hydroxyl group in EG by Lewis basic lattice oxygen on ZnO and/or N−H sites in 2-mIm promotes nucleophilic attack on this carbon center in urea toward cyclization for highly selective EC synthesis.

## 3. CONCLUSIONS

In this study, we demonstrated the application of a ZIF-derived Fe-doped ZnO catalyst in a highly selective EC synthesis through the efficient urea transesterification with EG. The Fe;ZnO−ZIF catalyst retains the characteristic structure of ZIF with a particle size of approximately 80 nm and contains highly dispersed ZnO particles with diameters of 2 nm accompanying the 2-mIm ligand near ZnO. Although the exact spatial distribution of Fe species in the STEM images obtained at the atomic scale was unclear because of the facile degradation of the catalyst upon exposure to the electron beam, we assume that ∼10 atom % of Fe could be successfully exchanged with Zn sites, resulting in the well-dispersed Zn and Fe phases. However, the XPS analysis results revealed that Fe doping induced the formation of oxygen vacancies and N−H from the remaining 2-mIm ligand on the catalyst surface, which led to the excellent conversion of EG into EC with high selectivity and improved TOF compared to the commercial ZnO and ZnO−ZIF. We suggest that this high catalytic performance toward EC synthesis can be ascribed to the synergistic effect between the Lewis acidic Zn and Lewis basic lattice O and N−H sites in Fe;ZnO−ZIF. We assume that these sites simultaneously contribute to the elaborate coordination of reaction intermediates within the micropores of ZIF-based catalysts involving EG, urea, and the catalytic surface. To facilitate the practical implementation of Fe;ZnO−ZIF in EC synthesis, it is essential to apply the Fe;ZnO−ZIF catalysts in a flow cell regime for cyclability, as well as to obtain more direct evidence elucidating the underlying synergistic mechanisms for further performance optimization. These aspects are currently under active investigation in our laboratory.

## 4. EXPERIMENTAL SECTION

**4.1. Chemicals.** For the synthesis of Fe;ZnO-ZIF, ethanol, methanol, 2-methylimidazole, $Zn(NO_3)_2{\cdot}6H_2O$, and $FeSO_4{\cdot}6H_2O$ were used, all of which were purchased from Sigma-Aldrich. Urea and ethylene glycol (EG) were used as reagents for the synthesis of ethylene glycol (EC) through transesterification of urea with EG. Also, both chemicals were purchased from Sigma-Aldrich. Phosphoric acid ($H_3PO_4$) was purchased from SAMCHUN PURE CHEMICAL. All chemicals were used as received. Deionized (DI) water (18.2 MΩ) was obtained from Direct-Q 5UV.

**4.2. Synthesis of Fe;ZnO-ZIF.** Fe;ZnO-ZIF was produced using the 1:1 (v:v) ethanol and methanol mixture. To a 600 mM solution of 2-methylimidazole was added with stirring a solution of 150 mM $Zn(NO_3)_2{\cdot}6H_2O$ containing 5 mM $FeSO_4{\cdot}6H_2O$. The stirring was continued for a short until the vortex was no longer visible and then stopped. The mixture


https://doi.org/10.1021/acsomega.3c05023
ACS Omega 2023, 8, 48704−48710

was left to stand under dark conditions at room temperature (RT) for 2 h. After 2 h, the catalyst was separated by centrifugation and washed using a 1:1 (v:v) ethanol and methanol mixture. After vacuum drying at 85 °C overnight, the catalyst was calcinated at 100 °C for 7 h and then at 350 °C for 2 h.

**4.3. Characterization.** A thermogravimetric analyzer (Discovery TGA 5500, TA Instruments) at the National Instrumentation Center for Environmental Management (NICEM) of Seoul National University (SNU) was used to determine the carbonization regime of the catalyst and confirm the thermal stability of the catalyst. A scanning electron microscope (SUPRA 55VP, Carl Zeiss) was utilized to confirm a rhombic dodecahedron like structure of Fe;ZnO-ZIF using an accelerating voltage of 2 kV at the NICEM of SNU. The transmission electron microscopic analysis at 300 kV (Themis Z, Thermo Fisher) was carried out at the Research Institute of Advanced Materials (RIAM) of SNU. At the same time, energy dispersive and electron energy loss spectroscopy (EELS) were also used to confirm the elements comprising Fe;ZnO-ZIF, such as Fe and Zn. Inductively coupled plasma (ICP)-mass spectroscopy (MS) was carried out using a Varian 820-MS instrument at NICEM of SNU to calculate the atomic ratio of Fe and Zn in Fe;ZnO-ZIF. For the preparation of the ICP-MS sample, Fe;ZnO-ZIF was dissolved in an aqua regia solution overnight and diluted 10-fold with deionized water for the analysis. The X-ray diffraction (XRD) patterns were obtained with an Ultima (IV) (Rigaku) instrument at the Yonsei Center for Research Facilities at Yonsei University. The chemical states of the Fe;ZnO-ZIF surface were analyzed by using an X-ray photoelectron spectrometer (K-alpha+, ThermoFisher Scientific) at Chung-Ang University. The TPD analysis was conducted at the Center for Material Characterization and Machining of Ajou University with an automated catalyst characterization system (AUTOCHEM II 2920, Micromeritics Instrument Corporation). For $CO_2$ and $NH_3$ TPD analysis, the samples were pretreated in an He flow (30 mL/min) at 150 °C for 2 h and were subsequently cooled to RT. For $CO_2$ TPD analysis, $CO_2$ was adsorbed in the quantitatively injected $CO_2$ (1 mL/pulse) every 2 min until two successive peaks were observed after the pretreatment. Then, He gas was flushed at RT for 90 min to remove the physisorbed $CO_2$ from the surface of the catalyst. Finally, desorption peaks were recorded by ramping the temperature to 450 °C with a rate of 10 °C/min and an He flow of 30 mL/min. In case of $NH_3$ TPD analysis, $NH_3$ (3% $NH_3$ in $N_2$) was quantitively injected (1 mL/pulse) every 2 min until more than two successive peaks appeared for adsorption of $NH_3$ on the catalyst surface after the pretreatment. Then, physisorbed $NH_3$ was removed with 90 min of He flush, which was the same condition as for the $CO_2$ TPD analysis. Lastly, we observed the $NH_3$ desorption by applying heat with a heating rate of 10 °C/min until the temperature reached 450 °C with a He flow rate of 30 mL/min.

**4.4. Synthesis of Ethylene Carbonate (EC).** Urea (0.3 mol), ethylene glycol (EG) (0.3 mol), and Fe;ZnO-ZIF (1 g) were sequentially placed in a three-neck round-bottom flask, which was then placed on a heating mantle. An acidic trap was connected to the flask to capture the $NH_3$ produced during the transesterification reaction. The reaction mixture was stirred at around 950 rpm while being heated to 160 °C under an applied vacuum at 160 mmHg. The application of vacuum was critical to achieve high conversion efficiency by continuous extraction of $NH_3$ gas in the reaction chambers, which led to a continuous forward reaction by Le Chatelier's principle. Heating was carried out for 150 min from the moment the sample reached 160 °C. The product was immediately transferred to a vial after the reaction was done.

**4.5. Selectivity and Turnover Frequency (TOF) Calculation.** Experimental data for the selectivity and TOF calculation were obtained from infrared spectroscopy and gas chromatography-MS investigation. Before the reaction product solidified, it was purified with a syringe filter and then the purified product was mixed with mono ethylene glycol. If the reaction product had solidified completely, then heat was applied to melt it.

## ■ ASSOCIATED CONTENT

### Supporting Information

The Supporting Information is available free of charge at https://pubs.acs.org/doi/10.1021/acsomega.3c05023.

Thermograms in TGA, EELS spectra, XRD pattern of Fe;ZIF, TPD profiles, schematic illustration of the reaction mechanism, conversion efficiencies by the reaction time, IR spectra of products after 150 and 240 min of reaction, GC spectrum for the reaction products, and table of selectivity toward EC synthesis (PDF)

## ■ AUTHOR INFORMATION


### Corresponding Author

**Sung Yul Lim** − *Department of Chemistry, College of Science, Kyung Hee University, Seoul 02447, Republic of Korea;* orcid.org/0000-0002-2838-6967; Email: limsy@khu.ac.kr

### Authors

**Sumin Lee** − *Department of Chemistry, College of Science, Kyung Hee University, Seoul 02447, Republic of Korea*

**Hyun Joo Lee** − *Department of Chemistry, College of Science, Kyung Hee University, Seoul 02447, Republic of Korea*

**Seung Hwan Chung** − *Department of Chemistry, College of Science, Kyung Hee University, Seoul 02447, Republic of Korea*

**Je Seung Lee** − *Department of Chemistry, College of Science, Kyung Hee University, Seoul 02447, Republic of Korea;* orcid.org/0000-0002-5033-7109

Complete contact information is available at: https://pubs.acs.org/10.1021/acsomega.3c05023


### Notes

The authors declare no competing financial interest.

## ■ ACKNOWLEDGMENTS

This work was supported by grants from the National Research Foundation of Korea funded by the Ministry of Science and ICT (NRF-2021R1C1C1012503, 2021R1A4A5032876, 2022K1A4A7A04095693, and 2021M3H7A1026180).

## ■ REFERENCES

(1) Ghiat, I.; Al-Ansari, T. A Review Of Carbon Capture and Utilization as a $CO_2$ Abatement Opportunity within the EWF Nexus. *J. CO2 Util.* **2021**, *45*, No. 101432.

(2) Piao, Z.; Gao, R.; Liu, Y.; Zhou, G.; Cheng, M. A Review on Regulating $Li^+$ Solvation Structures in Carbonate Electrolytes for Lithium Metal Batteries. *Adv. Mater.* **2023**, *35*, No. 2206009.
(3) Lee, K. M.; Jang, J. H.; Balamurugan, M.; Kim, J. E.; Jo, Y. I.; Nam, K. T. Redox-neutral Electrochemical Conversion of $CO_2$ to Dimethyl Carbonate. *Nat. Energy* **2021**, *6*, 733−741.
(4) Fakhrnasova, D.; Chimentao, R. J.; Medina, F.; Urakawa, A. Rational and Statistical Approaches in Enhancing the Yield of Ethylene Carbonate in Urea Transesterification with Ethylene Glycol over Metal Oxides. *ACS Catal.* **2015**, *5*, 6284−6295.
(5) Gregory, G. L.; Ulmann, M.; Buchard, A. Synthesis of 6-membered Cyclic Carbonates from 1,3-diols and Low $CO_2$ Pressure: A Novel Mild Strategy to Replace Phosgene Reagents. *RSC Adv.* **2015**, *5*, 39404−39408.
(6) Kamphuis, A. J.; Picchioni, F.; Pescarmona, P. P. $CO_2$-fixation into Cyclic and Polymeric Carbonates: Principles and Applications. *Green Chem.* **2019**, *21*, 406−448.
(7) Nasirov, F.; Nasirli, E.; Ibrahimova, M. Cyclic Carbonates Synthesis by Cycloaddition Reaction of $CO_2$ with Epoxides in the Presence of Zinc-containing and Ionic Liquid Catalysts. *J. Iran. Chem. Soc.* **2022**, *19*, 353−379.
(8) Ravi, S.; Puthiaraj, P.; Ahn, W. S. Cyclic Carbonate Synthesis from $CO_2$ and Epoxides over Diamine-functionalized Porous Organic Frameworks. *J. CO2 Util.* **2017**, *21*, 450−458.
(9) North, M.; Pasquale, R.; Young, C. Synthesis of Cyclic Carbonates from Epoxides and $CO_2$. *Green Chem.* **2010**, *12*, 1514−1539.
(10) Li, Q. B.; Zhang, W. Y.; Zhao, N.; Wei, W.; Sun, Y. H. Synthesis of Cyclic Carbonates from Urea and Diols over Metal Oxides. *Catal. Today* **2006**, *115*, 111−116.
(11) Jia, Y. C.; Lv, L.; Nie, Y. Y.; Jiao, L. Y.; Shen, W. H.; Zhu, Z. Q.; Fang, Y. J. Mechanically Mixed ZnO-$Al_2O_3$ Catalysts in the Synthesis of Propylene Carbonate via Alcoholysis of Urea. *Can. J. Chem. Eng.* **2021**, *99*, 374−382.
(12) Zhao, X. Q.; An, H. L.; Wang, S. F.; Li, F.; Wang, Y. J. Synthesis of Ethylene Carbonate from Urea and Ethylene Glycol over Zinc/iron Oxide Catalyst. *J. Chem. Technol. Biotechnol.* **2008**, *83*, 750−755.
(13) Park, K. S.; Ni, Z.; Cote, A. P.; Choi, J. Y.; Huang, R. D.; Uribe-Romo, F. J.; Chae, H. K.; O'Keeffe, M.; Yaghi, O. M. Exceptional Chemical and Thermal Stability of Zeolitic Imidazolate Frameworks. *Proc. Natl. Acad. Sci. U.S.A.* **2006**, *103*, 10186−10191.
(14) Linder-Patton, O. M.; de Prinse, T. J.; Furukawa, S.; Bell, S. G.; Sumida, K.; Doonan, C. J.; Sumby, C. J. Influence of Nanoscale Structuralisation on the Catalytic Performance of ZIF-8: A Cautionary Surface Catalysis Study. *CrystEngComm* **2018**, *20*, 4926−4934.
(15) Zak, A. K.; Razali, R.; Majid, W. H. A.; Darroudi, M. Synthesis and Characterization of a Narrow Size Distribution of Zinc Oxide Nanoparticles. *Int. J. Nanomedicine* **2011**, *6*, 1399−1403.
(16) Tu, Y.; Chen, S. Q.; Li, X.; Gorbaciova, J.; Gillin, W. P.; Krause, S.; Briscoe, J. Control of Oxygen Vacancies in ZnO Nanorods by Annealing and their Influence on ZnO/PEDOT:PSS Diode Behaviour. *J. Mater. Chem. C* **2018**, *6*, 1815−1821.


https://doi.org/10.1021/acsomega.3c05023
*ACS Omega* 2023, 8, 48704−48710